Supplementary information:

Ultrahigh carrier mobility contributes to remarkably enhanced thermoelectric performance in *n*-type PbSe

Yu Xiao,[a,*] Liqing Xu,[a] Tao Hong,[b] Haonan Shi,[b] Sining Wang,[b] Xiang Gao,[c] Xiangdong Ding[a], Jun Sun[a] and Li-Dong Zhao[b,*]

[a]*State Key Laboratory for Mechanical Behavior of Materials, Xi'an Jiaotong University, Xi'an 710049, China. Email: xiao_yu@xjtu.edu.cn;*

[b]*School of Materials Science and Engineering, Beihang University, Beijing 100191, China. Email: zhaolidong@buaa.edu.cn;*

[c]*Center for High Pressure Science and Technology Advanced Research (HPSTAR), Beijing 100094, China*

Experimental details

Material synthesis: Raw materials, Pb bulk (5N), Se chunk (4N), Sb bulk (5N), and Cu particles (4N) were loaded into silica tubes with nominal compositions, flame-sealed at a residual pressure below ~ 10^{-4} Torr, slowly heated to 1323 K in 24 h and maintained at this temperature for 10 h. The furnace was shut down and cooled to room temperature. The obtained ingots were ground into powders and sintered by spark plasma sintering (SPS-211Lx) at 873 K for 12 min under an axial compressive stress of 50 MPa, resulting in highly densified disk-shaped samples.

Structural characterization: The powder X-ray diffraction (PXRD) patterns were obtained with Cu Kα (λ=1.5418 Å) radiation in a reflection geometry on a diffractometer operating at 40 KV and 20 mA and equipped with a position-sensitive detector. The calculation of lattice parameter was performed on the PXRD data with software package Materials Analysis using Diffraction (MAUD). The transmission electron microscopy (TEM) and high-resolution TEM (HRTEM) image as well as the scanning transmission electron microscopy (STEM) ADF image were conducted using a JEM F200 with a Schottky hot field gun at 200 kV.

Bandgap measurements: Refined powder was used to measure the optical bandgap by Infrared Diffuse Reflection method with a Fourier Transform Infrared Spectrometer (IRAffinity-1S). The spectrum was collected in the mid-IR (5000~450 cm^{-1}) and the reflectance to absorption data was converted to estimate the band gap using Kubelka-Munk equation: $\alpha/S = (1-R^2)/(2R)$, where R, S and α are the reflectance, scattering and absorption coefficients, respectively.

Hall measurements: Hall coefficient (R_H) were measured with van der Pauw method, which was conducted in Lake Shore 8400 Series, Model 8404, USA, from 300 K to 773 K, using four probes to contact the corners of a square sample. The applied reversible magnetic field and current are 0.9 T and 20 mA, respectively. The sample size is 8mm×8mm with thickness around 0.7 mm. The carrier density (n_H) was obtained by $n_H = 1/(e \bullet R_H)$, and carrier mobility (μ_H) was calculated using the relationship $\mu_H = \sigma \bullet R_H$ with σ being the measured electrical conductivity.

Thermoelectric transport properties measurements: The obtained highly-

densified spark plasma sintering (SPS) processed pellets were cut into bars with dimensions around ~ 12×3×3 mm^3 for simultaneous measurement of the Seebeck coefficient and electrical conductivity using Cryoall CTA instrument under a low-pressure helium atmosphere from 300 to 873 K. The uncertainty of the Seebeck coefficient and electrical conductivity measurement was 5%. The SPS pellets were cut and polished into a disk-like shape with sizes of ~ 6 mm diameter and ~ 2 mm thickness for thermal diffusivity (D) measurements. The samples were coated with a thin layer of graphite to minimize errors from the emissivity method in Netzsch LFA457. The sample density (ρ) was determined using the dimensions and mass of the samples. The specific heat capacity (C_p) was estimated with the Debye model (see next section). The thermal diffusivity data was analyzed using a Cowan model with pulse correction. The uncertainty of the thermal conductivity was estimated to be within 8%, considering all the uncertainties from thermal conductivity, electrical conductivity and Seebeck coefficient. The combined uncertainty for all measurements involved in the calculation of ZT was less than 20%.

Heat capacity: The Debye model considers the individual contributions of phonons and effects of thermal expansion of lattice. The temperature-dependent total heat capacity ($C_{p,tot}$) can be obtained with following relationships:

$$C_{p,tot} = C_{p,ph}(T) + C_{p,D}(T)$$

where $C_{p,ph}$ and $C_{p,D}$ denote heat capacity originated from phonon and lattice dilation, respectively. The phonon heat capacity $C_{p,ph}$ can be calculated by:

$$C_{p,ph}(T/\Theta_D) = 9R\left(\frac{T}{\Theta_D}\right)^3 \int_0^{\Theta_D/T} \frac{x^4 e^x}{\left(e^x - 1\right)^2} dx$$

where Θ_D is Debye temperature, R is molar gas constant, $x=\hbar\omega/k_B T$, in which $\hbar$, ω and k_B denote Planck constant, phonon vibration frequency and Boltzmann constant, respectively.

The effects of lattice dilation on heat capacity $C_{p,D}$ can be obtained from:

$$C_{p,D}(T) = C_{ele,D}(T) + C_{ph,D}(T) = \frac{9BT\alpha^2}{10^6 \rho}$$

where B is the isothermal bulk modulus, α is the linear coefficient of thermal expansion, and ρ is sample density. Notably, the electron heat capacity is not taken into account due to its negligible effects on lattice dilation compared with phonon.

Lorenz number calculation: The Lorenz number (L) is used to evaluate the electronic thermal conductivity (κ_{ele}) with a relationship of $\kappa_{ele}=L\sigma T$, where the σ is the electrical conductivity, T denotes working temperature. The Lorenz number can be obtained by fitting the Seebeck coefficient to the reduced chemical potential with following equations:

$$L=\left(\frac{k_B}{e}\right)^2\left(\frac{\left(r+\frac{7}{2}\right)F_{r+\frac{5}{2}}(\eta)}{\left(r+\frac{3}{2}\right)F_{r+\frac{1}{2}}(\eta)}-\left[\frac{\left(r+\frac{5}{2}\right)F_{r+\frac{3}{2}}(\eta)}{\left(r+\frac{3}{2}\right)F_{r+\frac{1}{2}}(\eta)}\right]^2\right)$$

$$S=\pm\frac{k_B}{e}\left(\frac{\left(r+\frac{5}{2}\right)F_{r+\frac{3}{2}}(\eta)}{\left(r+\frac{3}{2}\right)F_{r+\frac{1}{2}}(\eta)}-\eta\right)$$

where the $F_n(\eta)$ is the n-th order Fermi integral:

$$F_n(\eta)=\int_0^\infty\frac{x^n}{1+e^{x-\eta}}dx$$

$$\eta=\frac{E_f}{k_BT}$$

where k_B is the Boltzmann constant, e is the electron charge and E_f denotes the Fermi level, r is the scattering factor, and the acoustic phonon scattering has been assumed as the main carrier scattering mechanism with r=-1/2.

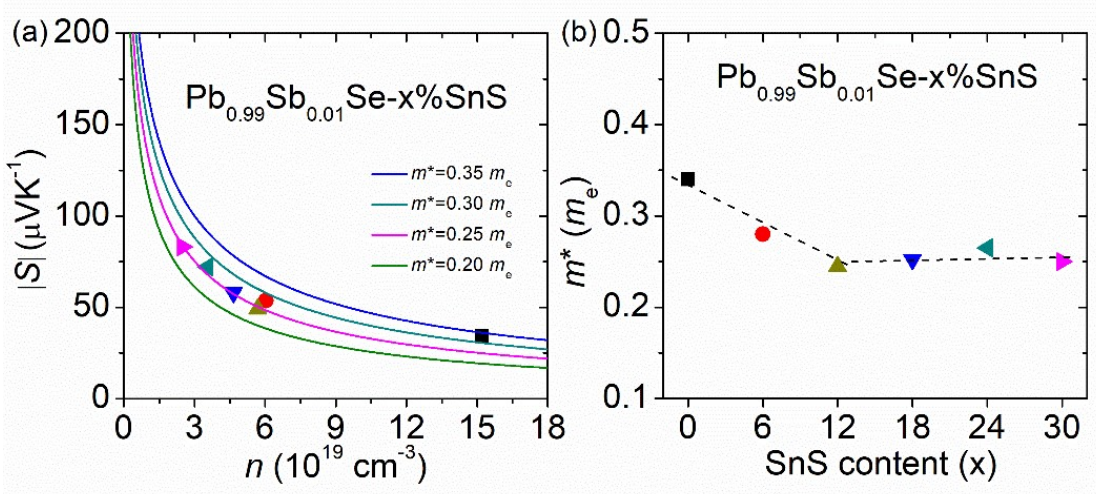

Figure S1. (a) Room-temperature Pisarenko relationship with effective mass, m^* = 0.20, 0.25, 0.30, 0.35 m_e; (b) room-temperature effective mass as a function of SnS content.

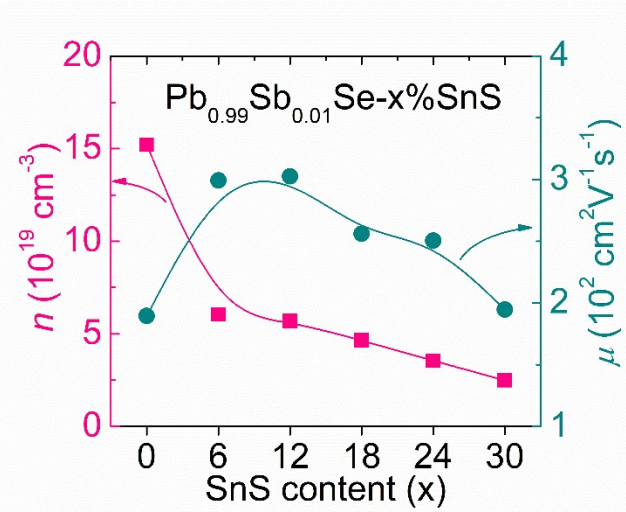

Figure S2. Carrier density and carrier mobility of $Pb_{0.99}Sb_{0.01}Se$-18%SnS as a function of SnS alloying content.

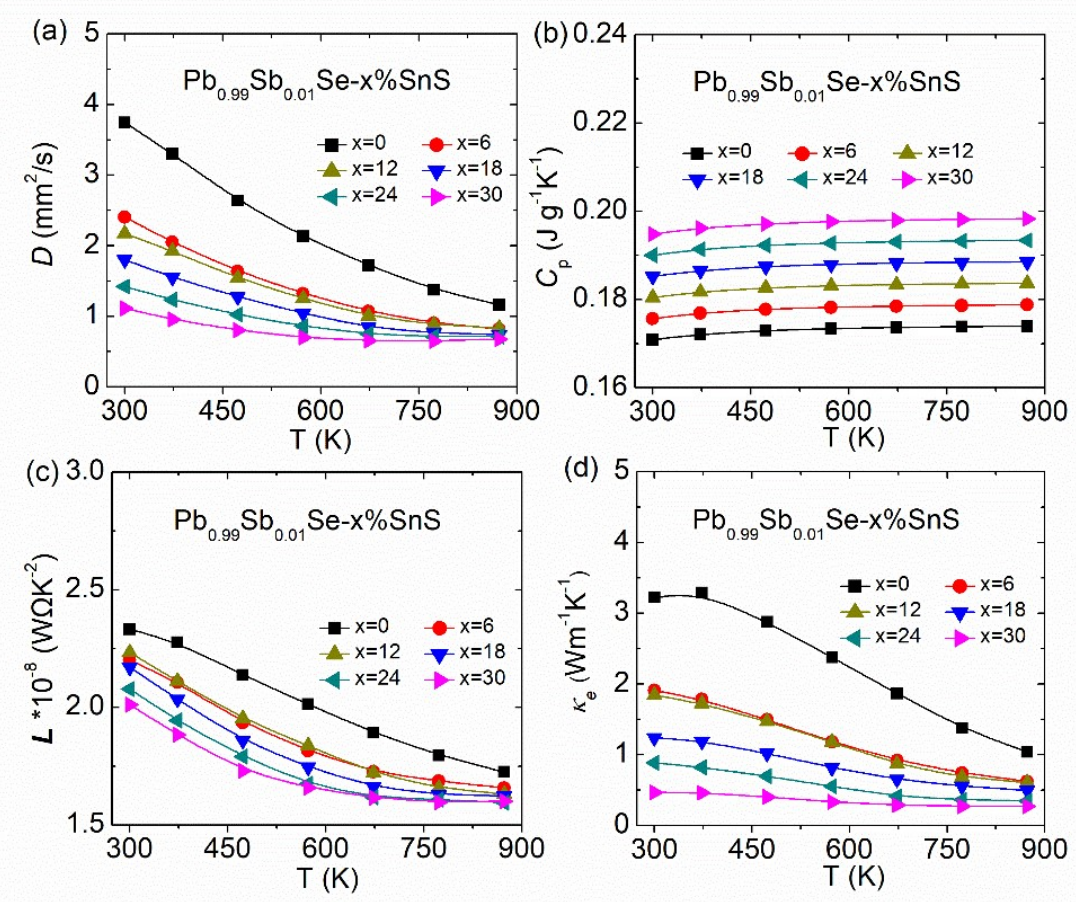

Figure S3. Temperature-dependent electrical transport properties for $Pb_{0.99}Sb_{0.01}Se$-x%SnS (x = 0-30): (a) thermal diffusivity; (b) heat capacity; (c) Lorenz number; (d) electronic thermal conductivity.

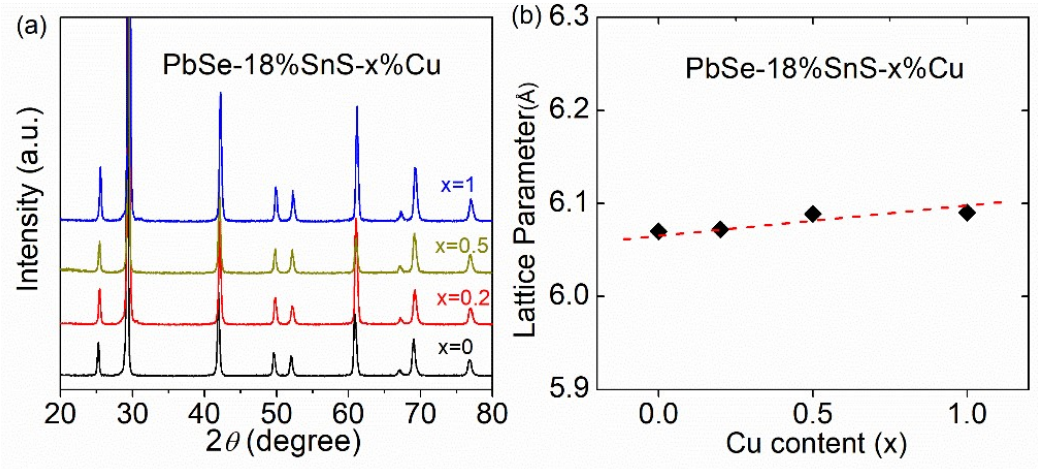

Figure S4. Phase analysis of PbSe-18%SnS-x%Cu (x = 0-1.0): (a) XRD patterns; (b) lattice parameter as a function of Cu content.

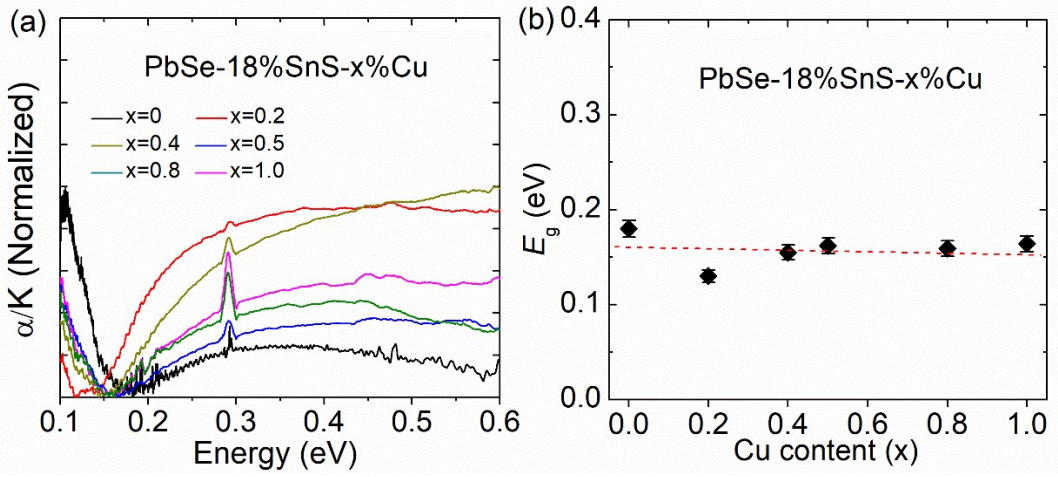

Figure S5. (a) Room-temperature optical spectrum of bandgap in PbSe-18%SnS-x%Cu (x=0-1.0); (b) fitted bandgap value as a function of Cu content.

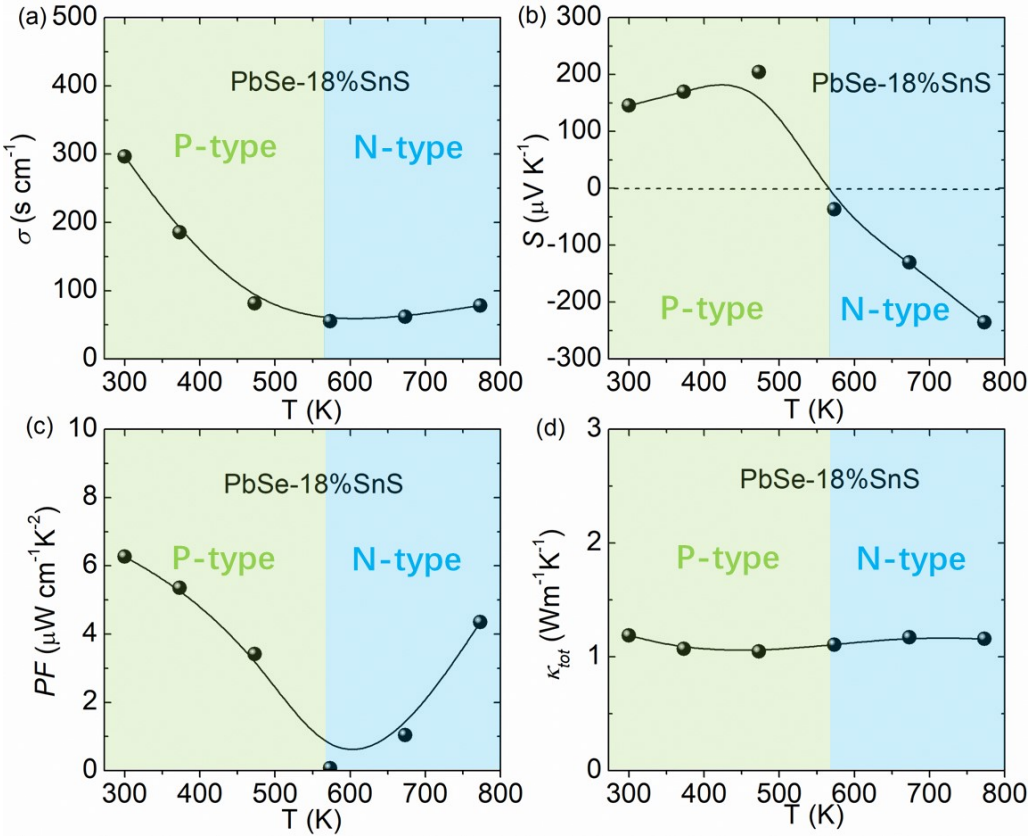

Figure S6. Thermoelectric transport properties as a function of temperature for $Pb_{0.99}Sb_{0.01}Se$-18%SnS: (a) electrical conductivity; (b) Seebeck coefficient; (c) power factor; (d) total thermal conductivity.

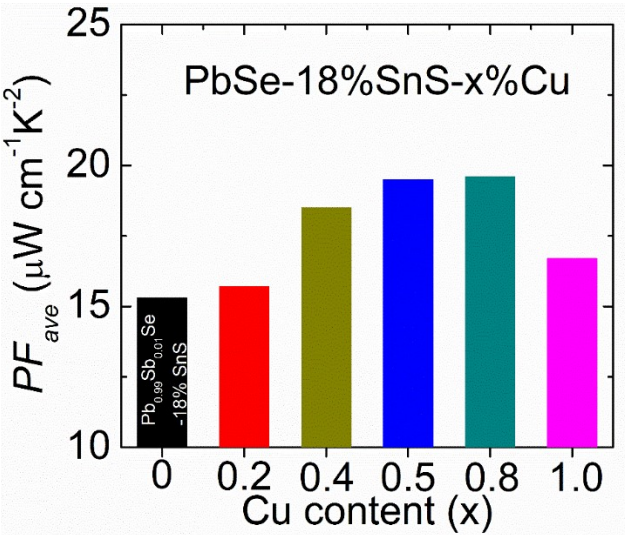

Figure S7. Comparison of power factor as a function of Cu content in PbSe-18%SnS-x%Cu (x = 0.2-1.0) and $Pb_{0.99}Sb_{0.01}Se$-18%SnS.

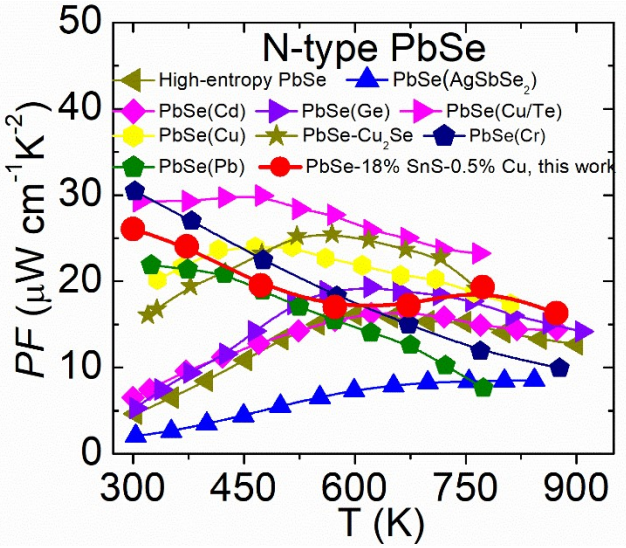

Figure S8. Comparison of power factor between this work and these high-performance *n*-type PbSe-based thermoelectric materials reported in previous works.

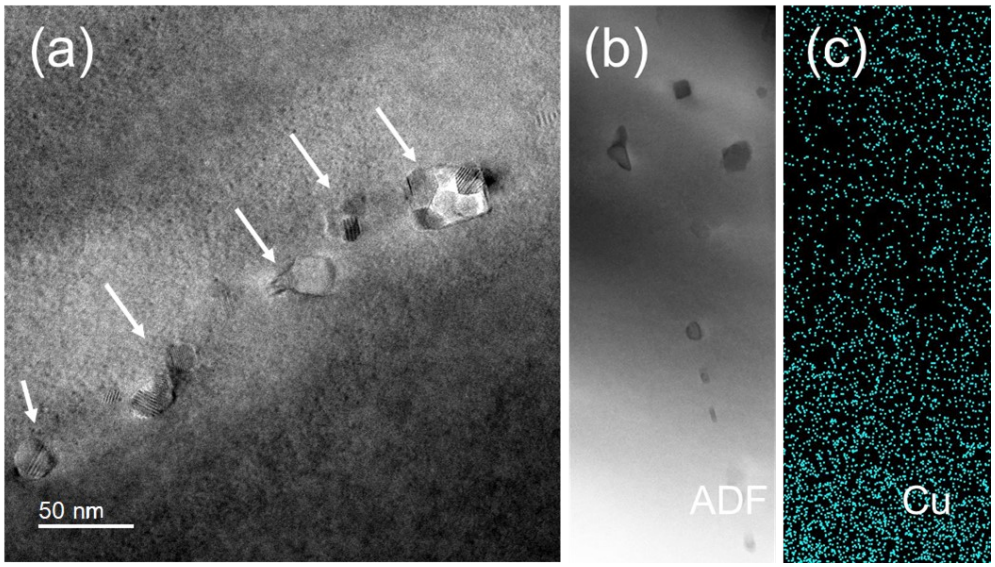

Figure S9. Micro/nanoscale SnS precipitates in PbSe-18%SnS-0.5%Cu. (a) High-magnification TEM image showing SnS nano-precipitates in the PbSe matrix; (b) STEM HAADF image; (c) Cu element mappings from EDS.

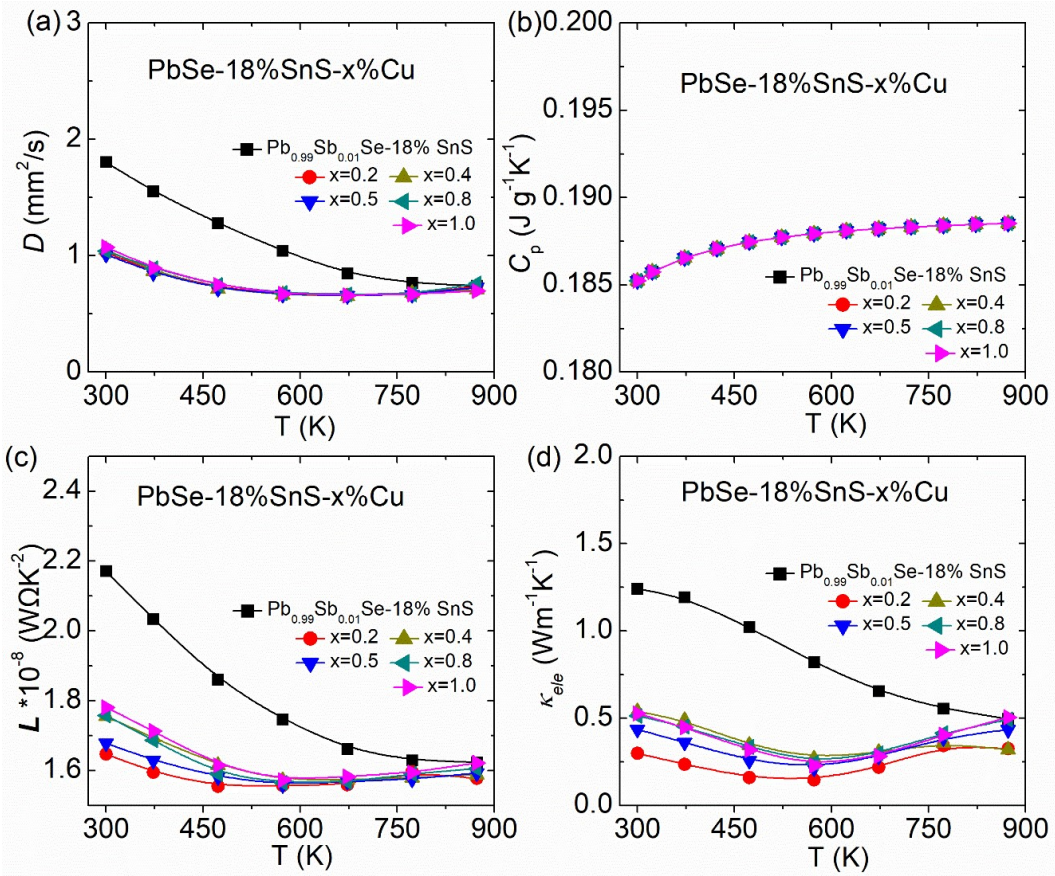

Figure S10. Comparison of temperature-dependent thermal transport properties of for PbSe-18%SnS-x%Cu (x = 0.2-1) and $Pb_{0.99}Sb_{0.01}Se$-18%SnS: (a) thermal diffusivity; (b) heat capacity; (c) Lorenz number; (d) electronic thermal conductivity.

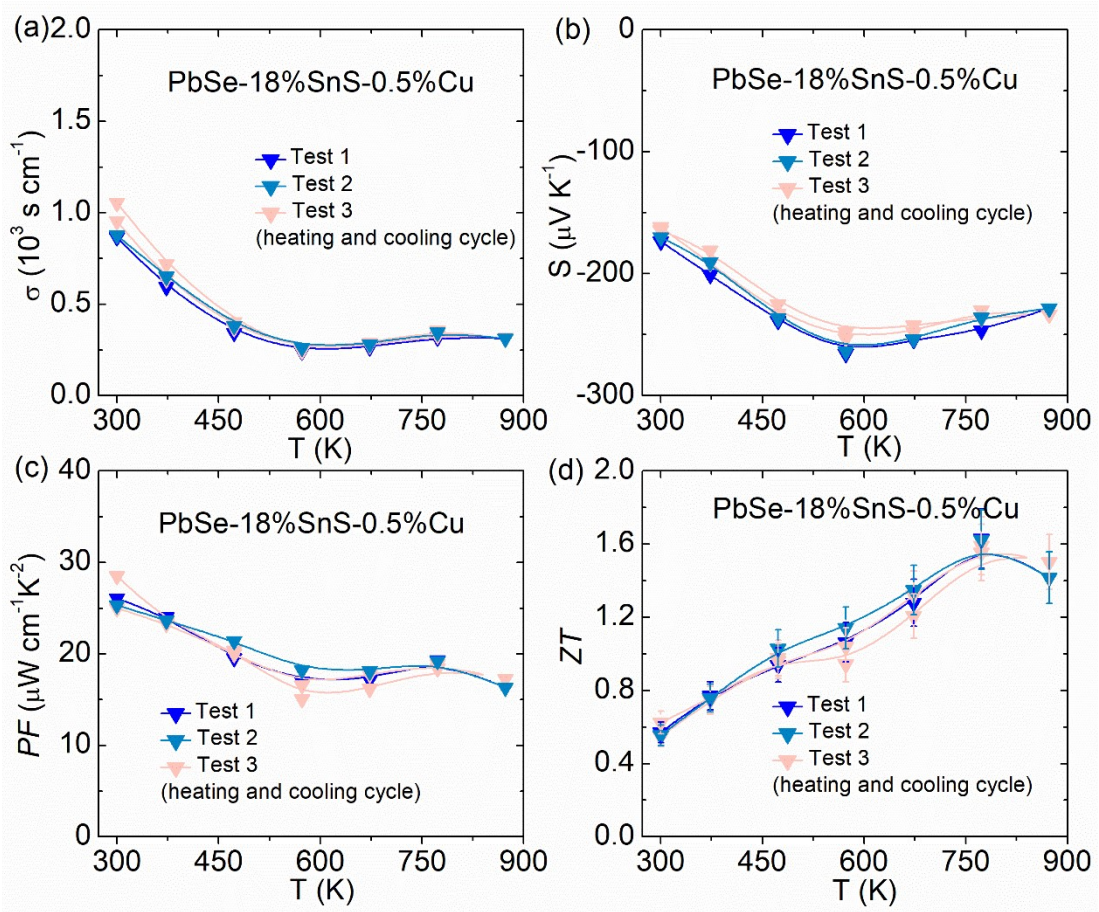

Figure S11. Cycle test of the thermoelectric transport properties in PbSe-18%SnS-0.5%Cu: (a) electrical conductivity; (b) Seebeck coefficient; (c) power factor; (d) *ZT* value.

Table S1. Room-temperature thermoelectric parameters in all samples in this work, including sample density (ρ), carrier density (n), carrier mobility (μ), total thermal conductivity (κ_{tot}) and ZT_{max} at working temperature range (300-873 K), the Hall measurements have been conducted for three times in PbSe-18%SnS-0.5%Cu to check its repeatability.

Samples	ρ (g cm^{-3})	n (10^{19}cm^{-3})	μ (cm^{-2}V^{-1}s^{-1})	κ_{tot} (Wm^{-1}K^{-1})	ZT_{max} (300-823 K)
$Pb_{0.99}Sb_{0.01}Se$	7.93	15.2 (n)	190	5.08	0.9
$Pb_{0.99}Sb_{0.01}Se$-6%SnS	7.75	6.04 (n)	299	3.28	1.1
$Pb_{0.99}Sb_{0.01}Se$-12%SnS	7.43	5.69 (n)	303	2.91	1.3
$Pb_{0.99}Sb_{0.01}Se$-18%SnS	7.30	4.65 (n)	256	2.44	1.31
$Pb_{0.99}Sb_{0.01}Se$-24%SnS	7.08	3.65 (n)	251	1.91	1.1
$Pb_{0.99}Sb_{0.01}Se$-30%SnS	6.94	2.49 (n)	195	1.50	1.0
PbSe-18%SnS	7.37	0.53 (p)	349	1.12	--
PbSe-18%SnS-0.2%Cu	7.35	0.08 (n)	4712	1.40	1.2
PbSe-18%SnS-0.4%Cu	7.33	0.13 (n)	4909	1.43	1.4
PbSe-18%SnS-0.5%Cu (1st)	7.31	0.089 (n)	6081	1.37	1.6
PbSe-18%SnS-0.5%Cu (2nd)	-	0.100 (n)	5412	-	-
PbSe-18%SnS-0.5%Cu (3rd)	-	0.094 (n)	5758	-	-
PbSe-18%SnS-0.8%Cu	7.36	0.14 (n)	4312	1.42	1.5
PbSe-18%SnS-1%Cu	7.38	0.11 (n)	5604	1.46	1.4